Unifying Advective and Diffusive Descriptions of Bedform Pumping in the Benthic Biolayer of Streams

Stanley B. Grant[1,2], Ahmed Monofy[3], Fulvio Boano[3], Jesus D. Gomez-Velez[4], Ian Guymer[5], Judson Harvey[6], Marco Ghisalberti[7]

[1]Occoquan Watershed Monitoring Laboratory, Department of Civil and Environmental Engineering, Virginia Tech, 9408 Prince William Street, Manassas VA 20110, USA

[2]Center for Coastal Studies, Virginia Tech, 1068A Derring Hall (0420), Blacksburg, VA 24061, USA

[3]Department of Environment, Land and Infrastructure Engineering, Politecnico di Torino, Torino 10129, Italy

[4]Department of Civil and Environmental Engineering, Vanderbilt University, Nashville, TN 37205, USA

[5]Department of Civil and Structural Engineering, Sir Frederick Mappin Building, Mappin Street, University of Sheffield, S1 3JD, England

[6]United States Geological Survey, Earth System Processes Division, Reston VA, 20192, USA

[7]Oceans Graduate School, University of Western Australia, Perth, WA, 6009, Australia.

Corresponding author: Stanley B. Grant (stanleyg@vt.edu)

- Parallel advective and diffusive models of solute transport through the benthic biolayer of streams by bedform pumping are derived
- The two models are functionally equivalent provided that the diffusion model's dispersion coefficient decays exponentially with depth
- Both frameworks closely reproduce measured patterns and rates of bedform pumping, and provide complementary predictive capabilities

Abstract. Many water quality and ecosystem functions performed by streams occur in the benthic biolayer, the biologically active upper (~5 cm) layer of the streambed. Solute transport through the benthic biolayer is facilitated by bedform pumping, a physical process in which dynamic and static pressure variations over the surface of stationary bedforms (e.g., ripples and dunes) drive flow across the sediment-water interface. In this paper we derive two predictive modeling frameworks, one advective and the other diffusive, for solute transport through the benthic biolayer by bedform pumping. Both frameworks closely reproduce patterns and rates of bedform pumping previously measured in the laboratory, provided that the diffusion model's dispersion coefficient declines exponentially with depth. They are also functionally equivalent, such that parameter sets inferred from the advective model can be applied to the diffusive model, and vice versa. The functional equivalence and complementary strengths of these two models expands the range of questions that can be answered, for example by adopting the advective model to study the effects of geomorphic processes (such as bedform adjustments to land use change) on flow-dependent processes, and the diffusive model to study problems where multiple transport mechanisms combine (such as bedform pumping and turbulent diffusion). By unifying advective and diffusive descriptions of bedform pumping, our analytical results provide a straightforward and computationally efficient approach for predicting, and better understanding, solute transport in the benthic biolayer of streams and coastal sediments.

Plain Language Summary

How far and fast pollutants travel downstream is often conditioned on what happens in a thin veneer of biologically active bottom sediments called the benthic biolayer. However, before a pollutant can be removed in the benthic biolayer it must first be transported across the sediment-water interface and through the interstitial fluids of these surficial sediments. In this paper we demonstrate that one important mechanism for transporting solutes to, and through, the benthic biolayer—bedform pumping—can be interchangeably represented as either a two-dimensional advective process or a one-dimensional dispersion process. The complementary nature of these models expands the range of benthic biolayer processes that can be studied and predicted with the end goal of improving coastal and stream water quality.

1. Introduction

The movement of water into and out of the hyporheic zone, or "hyporheic exchange", occurs over a wide range of spatial (and temporal) scales, from >10 km (>1 year) to <1 m (<1 hr) (Boano et al., 2014; Gomez-Velez and Harvey, 2014; Wörman et al., 2007). This $>10^3$ range of temporal and spatial scales raises trade-offs—relative to residence times, reaction times, and exchange rates—that can influence the hyporheic zone's ability to process nutrients and other pollutants (Harvey et al., 2013). For example, Gomez-Velez et al. (2015) evaluated the residence time/exchange rate trade-off for aerobic respiration and denitrification in the Mississippi River Network, calculating for each reach a so-called Reaction Significance Factor, RSF (Harvey et al., 2013). In the RSF framework, more nutrients are removed when hyporheic zone residence times are comparable to reaction times and the uptake length is short compared to the reach length (i.e., the RSF is large). These authors found that the smallest scales of hyporheic exchange are the most important for nutrient processing in streams, with RSFs consistently larger for vertical exchange over submerged ripples and dunes (length-scales of the order of 10^0 m) compared to lateral exchange over larger geomorphic features such as river bars and meandering banks (length-scales of the order of 10^2 to 10^3 m). This conclusion, which is based on physical arguments, is reinforced by findings that microbial biomass and nitrification and denitrification potential tend to be concentrated in the upper 5 cm of the streambed, a region of the hyporheic zone known as the "benthic biolayer" (Tomasek et al., 2018; Knapp et al., 2017; Caruso et al., 2017). Collectively, these results underscore the importance of elucidating physical mechanisms responsible for hyporheic exchange at the scale where nutrient transformations primarily occur; that is, in the benthic biolayer.

79 At the scale of the benthic biolayer one important driver of hyporheic exchange is
80 bedform pumping, which occurs when dynamic and static pressure variations over the surface of
81 bedforms (e.g., ripples and dunes) drive flow across the sediment-water interface (SWI) in
82 spatially isolated upwelling and downwelling zones (Azizian et al., 2015; Azizian et al., 2017;
83 Grant et al., 2012; Grant et al., 2014; Fleckenstein et al., 2010; Cardenas et al., 2008; Elliot and
84 Brooks, 1997a,b; Thibodeaux and Boyle, 1987) (**Figure 1a**). Since its discovery in 1987
85 (Thibodeaux and Boyle, 1987), a number of analytical models have been proposed to describe
86 bedform pumping and its influence on stream water quality (reviewed in Boano et al., 2014).
87 Generally, these models can be grouped depending on whether they conceptualize bedform
88 pumping as an advective or diffusive process. Advective models are notable for their relatively
89 faithful representation of the laminar flow fields generated by bedform pumping (Elliott and
90 Brooks 1997a,b). An advantage of diffusive models is their ability to incorporate multiple
91 mechanisms for mass transport across the SWI (i.e., not just bedform pumping) including
92 molecular diffusion, turbulent diffusion and dispersion (Voermans et al., 2017; Voermans et al.,
93 2018; Grant et al., 2018a; Grant et al., 2018b; Grant et al., in review).
94 As commonly implemented, both types of analytical models rely on multiple assumptions
95 that limit their practical utility: (1) solute concentration in the overlying water column is assumed
96 constant in time; (2) two-way coupling across the SWI—whereby mass transfer out of the
97 streambed alters mass concentration in the overlying water column which, in turn, alters mass
98 transfer into the streambed, and so on—is not accounted for; (3) diffusive mixing in the
99 streambed is constant in depth, while the interstitial flow field generated by bedform pumping

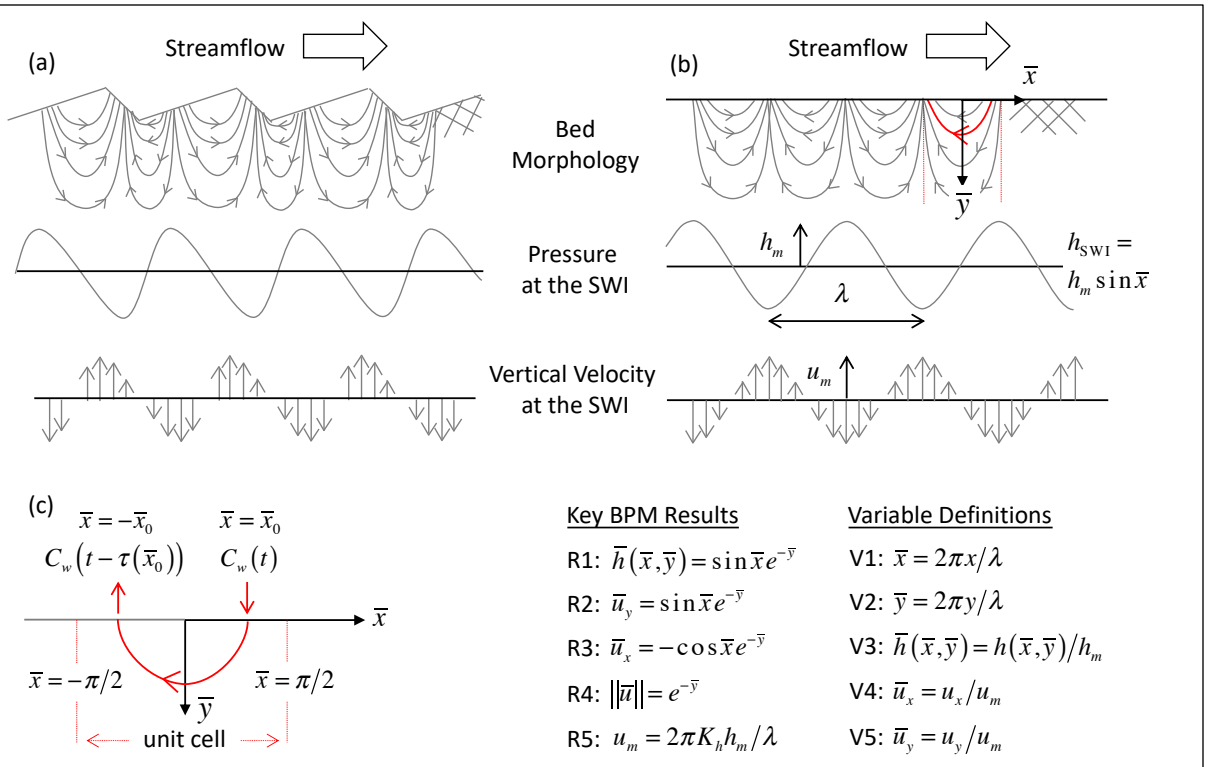

Figure 1. (**a**) Conceptual diagram of hyporheic exchange induced by advective flow across stationary bedforms. Shown are bedform morphology, streamlines through the sediment, pressure variation over the surface of the SWI, and upwelling and downwelling zones (upward and downward facing arrows). (**b**) A simplified analytical model of this process, the bedform pumping model (BPM), assumes a sinusoidal pressure head variation over a flat SWI. Streamlines through the sediment consist of repeating identical (or mirror image) unit cells (a single unit cell is indicated by the two red vertical dotted lines). (**c**) Blow-up of the unit cell extending from $\bar{x} = -\pi/2$ to $\bar{x} = \pi/2$. Each streamline in the unit cell is uniquely identified by where it enters the sediment at $\bar{x} = \bar{x}_0$, $0 < \bar{x}_0 < \pi/2$. Shown are the solute concentrations at the entrance, $C_w(t)$, and exit, $C_w(t - \tau(\bar{x}_0))$, points of a single streamline, where $\tau(\bar{x}_0)$ is the residence time of the streamline that enters the sediment at $\bar{x} = \bar{x}_0$.

100 decays exponentially (Elliott and Brooks, 1997a); and (4) some published diffusive models fail
101 to account for the finite porosity of the streambed, a violation of mass balance that can bias
102 estimates of the diffusivity downwards by a factor of ten (Grant et al., 2012).

In this paper we derive two parallel analytical frameworks, one advective and the other diffusive, that collectively address the model limitations noted above. The paper is organized as follows. In **Section 2** we review a canonical analytical model for advective bedform pumping originally developed by Elliott and Brooks (1997a,b) (**Section 2.1**), show that its residence time distribution closely follows the extreme value Fréchet distribution (**Section 2.2**), and derive from this result a set of fully coupled solutions for the evolution of solute concentration in the water and sediment columns of a closed system (**Section 2.3**). In **Section 3** we derive a parallel diffusive analytical framework for bedform pumping (**Section 3.1**), show how the choice of a diffusivity profile (constant or exponentially declining) leads to different Green's function (Leij et al., 2000) representations of mass transport in the streambed (**Section 3.2**), and then derive from these Green's functions a set of fully coupled solutions for the evolution of solute concentration in the water and sediment columns of a closed system (**Section 3.3**). We test these models against previously published measurements of unsteady solute transport across artificial and natural bedforms in a recirculating flume (**Section 4**). Discussion of these results are presented in **Section 5** and conclusions in **Section 6**.

2. Advective Bedform Pumping Model (BPM)

2.1 Canonical Solution by Elliott and Brooks (EB)

A canonical advective model of bedform pumping (originally solved by Vaux (1968) and expanded on by Elliott and Brooks (1997a,b)), hereafter referred to as the bedform pumping model (**BPM**), assumes that hyporheic exchange is driven by a sinusoidal variation of pressure head over a flat SWI (**Figure 1b**). The wavelength λ [L] of the pressure wave corresponds to the wavelength of the bedform, and the trough and peak of the pressure wave correspond to where the velocity boundary layer detaches (at the bedform crest) and reattaches (on the lee side of the

bedform), respectively (Cardenas and Wilson, 2007a,b; Sawyer and Cardenas, 2009). If the hydraulic conductivity K_h [L T^{-1}] and porosity θ of the streambed are constant, Darcy's Law and the continuity equation can be jointly solved to yield the BPM's well-known formulae for the two-dimensional pressure head distribution and velocity field in the interstitial pores of the hyporheic zone (equations (R1) - (R5), **Figure 1b**) (Elliot and Brooks 1997a,b).

As documented in Supplemental Information (**Text S1**), if the sediment bed is initially solute free (at $\bar{t}=0$) and the solute in question is conservative (i.e., inert and does not adsorb to sediments) the average interfacial flux, $J(\bar{t})$ [M L^{-2} T^{-1}], of mass into the streambed can be represented as a convolution over all past water column concentrations, $C_w(\bar{t})$ [M L^{-3}]:

$$J(\bar{t})=\frac{u_m}{\pi}\left[C_w(\bar{t})-\int_0^{\bar{t}} C_w(\bar{t}-\bar{\tau})f_{\mathrm{RTD}}(\bar{\tau})d\bar{\tau}\right] \quad (1a)$$

$$f_{\mathrm{RTD}}(\bar{\tau})=\frac{\sin\left[\bar{x}_0(\bar{\tau})\right]\cos\left[\bar{x}_0(\bar{\tau})\right]}{1+\bar{x}_0(\bar{\tau})\tan\left[\bar{x}_0(\bar{\tau})\right]} \quad (1b)$$

$$\bar{\tau}=\frac{\bar{x}_0(\bar{\tau})}{\cos\left[\bar{x}_0(\bar{\tau})\right]} \quad (1c)$$

The function $f_{\mathrm{RTD}}(\bar{\tau})$ [-] is the probability density function (PDF) form of the BPM's residence time distribution (RTD), defined such that the quantity $f_{\mathrm{RTD}}(\bar{\tau})d\bar{\tau}$ is the fraction of water circulating through the hyporheic zone with dimensionless residence times in the range $\bar{\tau}$ to $\bar{\tau}+d\bar{\tau}$. The variable u_m appearing on the right hand side of equation (1a) is the maximum Darcy flux of water across the SWI, and time and residence time ($\bar{t}=t/t_T$ and $\bar{\tau}=\tau/t_T$, respectively) have been scaled by a characteristic timescale for the transport of solute through a bedform: $t_T=\lambda\theta/\pi u_m$ (all BPM variables defined in **Figure 1**).

2.2. The Fréchet Distribution and the BPM's Residence Time Distribution (RTD)

For any choice of the dimensionless residence time $\bar{\tau}$, numerical evaluation of the BPM's RTD requires two steps. First, the dimensionless starting position, $\bar{x}_0(\bar{\tau})$ [-], of the streamline in the unit cell with dimensionless time $\bar{\tau}$ (see **Figure 1c**) is obtained by numerically solving the implicit expression for $\bar{x}_0(\bar{\tau})$ (equation (1c)). This estimate of $\bar{x}_0(\bar{\tau})$ is then substituted into the RTD formula (equation (1b)) to obtain the fraction of flow leaving the hyporheic zone with that dimensionless residence time. Because hyporheic zone residence times vary over many orders of magnitude, it is convenient to divide the unit area under the RTD into evenly spaced logarithmic increments of dimensionless residence time (Azizian et al., 2017):

$$f_{\mathrm{RTD}}\left(\log_{10}\bar{\tau}\right)=\frac{dF_{\mathrm{RTD}}}{d\log_{10}\bar{\tau}}=2.303\bar{\tau}f_{\mathrm{RTD}}\left(\bar{\tau}\right) \tag{2a}$$

$$F_{\mathrm{RTD}}\left(\bar{\tau}\right)=1-\cos\left[\bar{x}_0\left(\bar{\tau}\right)\right] \tag{2b}$$

The cumulative distribution function (CDF) form of the RTD appearing in equation (2b), $F_{\mathrm{RTD}}(\bar{\tau})$ [-], is defined as the fraction of water circulating through the hyporheic zone with dimensionless residence time of $\bar{\tau}$ or younger; the PDF and CDF forms of the RTD are related in the usual way: $f_{\mathrm{RTD}}(\bar{\tau})=dF_{\mathrm{RTD}}(\bar{\tau})/d\bar{\tau}$. As demonstrated in the Supplemental Information (**Text S2**), our definition of $F_{\mathrm{RTD}}(\bar{\tau})$ is mathematically consistent with the one derived by Elliott and Brooks (hereafter, **EB**) in their original publication of the BPM (Elliott and Brooks, 1997a).

The BPM's RTD spans a thousand-fold change in dimensionless residence times, from $\bar{\tau}<0.1$ to $\bar{\tau}>100$ (black curves in **Figures 2a** and **2b**). It is well described by both the Fréchet and Pareto distributions, reasonably well described by the Log-Normal distribution, and poorly described by the Gamma and Exponential distributions (colored curves in the figure). The

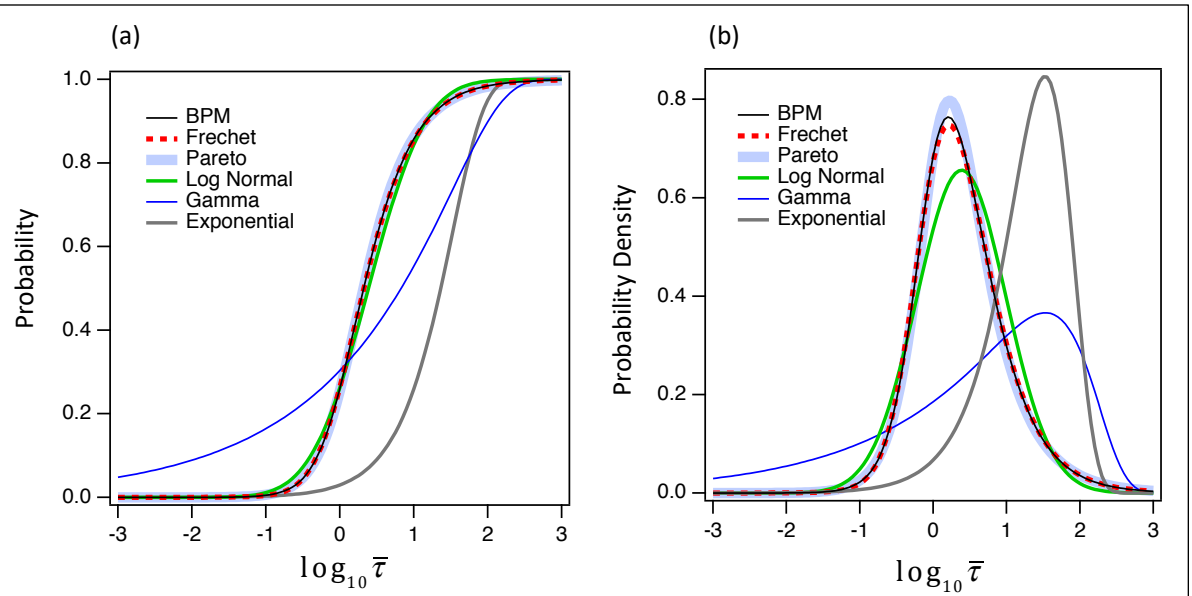

Figure 2. (**a**) CDF representation of the BPM's RTD (thin black curve) plotted against log-transformed dimensionless residence time. Optimized CDFs for five other probability distributions are shown. These five distributions were optimized by randomly sampling the BPM's RTD 10,000 times and employing maximum likelihood estimation to infer distribution parameter values from these realizations. (**b**) The PDF form of the same distributions shown in (a). The vertical axis represents the change in probability density per (base 10) logarithmic change in dimensionless residence time, $f_{\mathrm{RTD}}\left(\log_{10}\overline{\tau}\right)$ (see equation (2a) and discussion thereof). The mathematical definition of these distributions and their inferred parameter values are summarized in **Table 1**.

remarkable similarity between the BPM's RTD and the Fréchet distribution—a heavy-tailed extreme value distribution (Kotz and Nadarajah, 2000)—has not, to our knowledge, been noted in the literature. More commonly, the power-law or Pareto distribution is adopted to represent hyporheic exchange (Bottacin-Busolin and Marion, 2010). However, the three-parameter version of the Pareto distribution was required to obtain a reasonable match to the BPM's RTD and, even then, the Pareto distribution ranked second behind the (two-parameter) Fréchet distribution (see Kolmogorov-Smirnov ranking in **Table 1**). The log-normal distribution, which is sometimes used to model residence times in the hyporheic zone (e.g., Wörman et al., 2002; Azizian et al.,

2017), underpredicts the RTD's heavy tail but is otherwise comparable to the BPM's RTD (compare green and black curves, **Figure 2b**). The Gamma distribution has been used to represent the RTD of water parcels moving through hillslopes (Kirchner et al., 2000; Leray et al., 2016) while the Exponential RTD underpins the Transient Storage Model, a popular hyporheic exchange modeling framework (Knapp and Kelleher, 2020)). Based on the results in **Figure 2** these last two distributions should not be used to represent the BPM's RTD. For the analysis that follows we adopted the optimized Fréchet distribution in place of the BPM's RTD for three reasons: (1) the Fréchet distribution is parsimonious and closely matches the BPM's actual RTD (**Table 1** and **Figure 2**); (2) this approach side steps the numerical challenges associated with the two-step process required to solve the BPM's RTD (see equation (1b) and discussion thereof); and, (3) the Laplace Transform of the Fréchet distribution can be computed analytically, which simplifies the mass balance analysis described next.

2.3 Unsteady Solute Concentration in the Water Column of a Closed System

An example of bedform pumping in a closed system is the recirculating flume set-up illustrated in **Figure 3a**. A mass M of a conservative solute is added to the water column of a solute-free recirculating flume at time $t=0$. After a short mixing period, the concentration in the water column is approximately $C_0 = M/V_w$ where V_w is the volume of water above the sediment bed and in the recirculating pipes. At this point in time, the second term on the right hand side of equation (1a) is negligible (because no solute has yet passed through the hyporheic zone and returned to the stream) and therefore the BPM predicts that the initial flux of solute into the bed should be: $J_0 = C_0 u_m / \pi$. With increasing elapsed time ($t>0$) the solute concentration in the overlying water column declines (**Figure 3b**), the integral term in equation (1a) becomes progressively larger in magnitude (as solute in the streambed begins to return to the stream), and the net flux across the

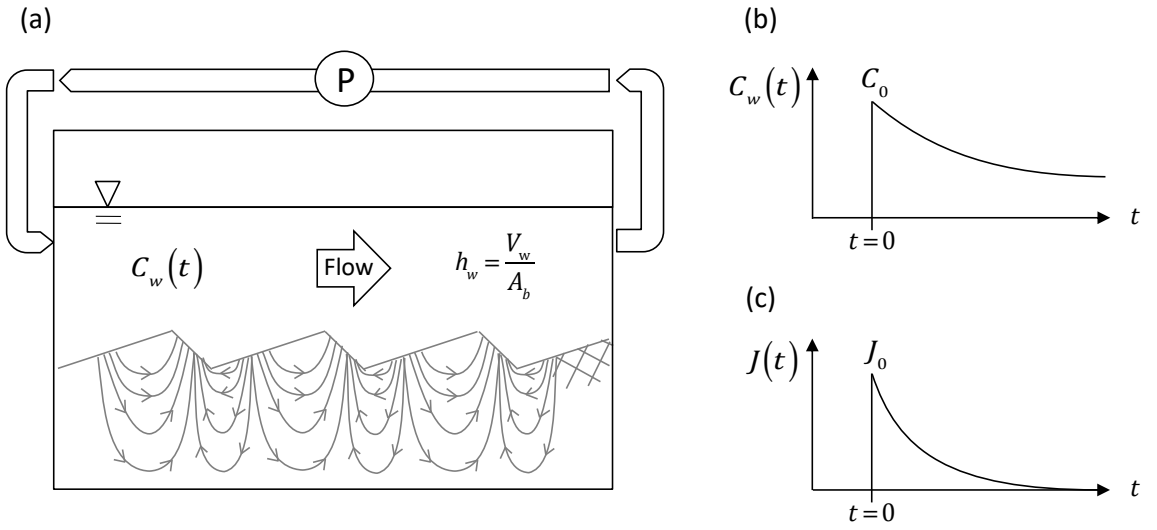

Figure 3. (**a**) A conceptual diagram of a recirculating flume experiment, in which streamflow over the top of stationary bedforms induces bedform pumping and hyporheic exchange. The water column has an "effective depth" h_w equal to the total volume V_w of water above the SWI and in the recirculation pipes divided by the area of the SWI A_b. (**b**) In a typical step-change experiment, the concentration of a conservative solute in the overlying water column $C_w(t)$ is increased suddenly to C_0 at time $t=0$, and is everywhere equal to zero for $t<0$. Mixing across the SWI causes $C_w(t)$ to decline toward an equilibrium value. (**c**) Mass flux across the SWI $J(t)$ also increases to a maximum of J_0 at time $t=0$, and then declines toward zero over time.

197 SWI asymptotically approaches zero (**Figure 3c**). In practice, if the experiment runs long
198 enough, the water column solute concentration will approach an equilibrium value, C_{eq} [M L^{-3}],
199 reflecting a well-mixed final state in which the solute concentration is the same everywhere in
200 the overlying water column and the interstitial fluids of the sediment bed:

201 $$\bar{C}_{eq} = C_{eq} / C_0 = 1 / \left(d_b \theta / h_w + 1 \right) \quad (3)$$

New variables in equation (3) include the effective water depth h_w [L] (equal to the volume of water V_w [M L^{-3}] in the overlying water column and recirculating pipes divided by the surface area A_b [L^2] of the bed, $h_w = V_w / A_b$), sediment bed depth d_b [L] and porosity θ [-]. As the BPM assumes the streambed is infinitely deep, this analytical model never achieves equilibrium.

One challenge associated with deriving a solution for the recirculating flume problem illustrated in **Figure 3a** is the two-way coupling of solute concentrations above and below the SWI. This two-way coupling is evident when mass balance is performed over the recirculating flume's water column:

$$\frac{T}{t_T}\frac{d\overline{C}_w}{d\overline{t}} = -\overline{C}_w\left(\overline{t}\right) + \int_0^{\overline{t}} \overline{C}_w\left(\overline{t}-\overline{\tau}\right) f_{\mathrm{RTD}}\left(\overline{\tau}\right) d\overline{\tau} \qquad (4)$$

Here, the water column concentration has been scaled by its initial concentration at $t = 0$ ($\overline{C} = C / C_0$) and the variable $T = h_w \pi / u_m$ represents a characteristic timescale for all water in the overlying water column and recirculating pipes to undergo hyporheic exchange. Two-way coupling manifests mathematically as a dependence of the time rate of change of the water column solute concentration (left hand side of equation (4)) on the entire past history of water column solute concentration filtered through the hyporheic zone's RTD (convolution integral on the right hand side of equation (4)). In addition to providing an elegant interpretation of two-way coupling, the convolution representation of hyporheic exchange flux permits an analytical solution to the overall mass balance problem. This is because the Laplace Transform of a convolution of two variables is equal to the product of their respective Laplace Transforms (Graff, 2004). Thus, after applying the Laplace Transform to equation (4), solving for the solute concentration in the water column becomes a simple algebraic exercise:

$$\bar{C}_w\left(\bar{t}\right)=\mathcal{L}^{-1}\left[\frac{\bar{T}}{\bar{s}\bar{T}+1-\tilde{f}_{\mathrm{RTD}}\left(\bar{s};\beta,\mu\right)}\right] \tag{5a}$$

Here, the variable $\bar{T}=T/t_{\mathrm{T}}$ is a dimensionless timescale for hyporheic zone processing of water above the streambed, $\bar{s}=st_T$ is a dimensionless form of the Laplace transform variable and the symbol $\mathcal{L}^{-1}\left[\bullet\right]$ denotes the inverse Laplace Transform which, in practice, is solved numerically (see **Section 4.1**). The Laplace Transform of the Fréchet distribution can be computed analytically by applying the Right Shift rule (Graf, 2004) where $K_1\left(\bullet\right)$ is the modified Bessel function of the second kind and u is a dummy integration variable:

$$\tilde{f}_{\mathrm{RTD}}\left(\bar{s};\beta,\mu\right)=\frac{e^{\mu\bar{s}}}{1-e^{-\beta/\mu}}\left(2\sqrt{\beta\bar{s}}K_1\left(2\sqrt{\beta\bar{s}}\right)-\beta\int_0^{\mu}e^{-\bar{s}u}\frac{e^{-\beta/u}}{u^2}du\right) \tag{5b}$$

Because the Fréchet distribution parameters (β, μ) are known (see **Table 1**), we can infer from equation (5a) that $\bar{C}_w\left(\bar{t}\right)$ depends on a single dimensionless parameter, $\bar{T}=T/t_{\mathrm{T}}$. The two timescales appearing in this dimensionless parameter depend on physical characteristics of the recirculating flume as follows:

$$t_T=\frac{\lambda^2\theta}{2\pi^2K_hh_m} \tag{6a}$$

$$T=\frac{h_w\lambda}{2K_hh_m} \tag{6b}$$

Therefore, implementation of this analytical solution requires knowledge of the bedform wavelength λ, streambed porosity θ, streambed hydraulic conductivity K_h, the effective depth of the water column (taking into account the water in the recirculating system for the system illustrated in **Figure 3a**) h_w, and the half-amplitude of the pressure head variation h_m. With the

exception of h_m, these parameters are readily measured or predicted (e.g., the hydraulic conductivity can be estimated from the median grain diameter of unconsolidated sediments, for example using the Kozeny-Carman equation (McCabe et al. 2010)). To estimate h_m, the widely cited empirical formula proposed by EB (based on pressure measurements over a triangular bedform reported by Fehlman (1985)) can be employed:

$$h_m = 0.28\frac{V^2}{2g}\left(\frac{H/d}{0.34}\right)^{\gamma} \tag{7}$$

The variables V [L T^{-1}] and d [L] represent, respectively, the average velocity and depth of the overlying stream, H [L] is bedform height, and the empirical exponent is taken as either $\gamma = 3/8$ (if $H/d < 0.34$) or $\gamma = 3/2$ (if $H/d \geq 0.34$). The value of the multiplicative constant (0.28) on the right hand side of equation (7) can be adjusted depending on the height-to-wavelength ratio of the bedform (Shen et al., 1990; Fox et al., 2014).

2.4 Unsteady Interstitial Solute Concentration in the Sediment Column of a Closed System

A corresponding analytical solution can be derived for the spatiotemporal evolution of solute concentration in the interstitial fluids of the sediment bed. The solution is premised on the idea that the interstitial concentration of a conservative solute at any dimensionless time $\bar{t}$ is equal to the concentration that was present in the water column some location-dependent dimensionless residence time ago: $\bar{C}_s\left(\bar{x},\bar{y},\bar{t}\right) = \bar{C}_w\left(\bar{t} - \bar{\tau}\left(\bar{x},\bar{y}\right)\right)$. New variables appearing here include the dimensionless interstitial solute concentration, $\bar{C}_s = C_s\left(\bar{x},\bar{y},\bar{t}\right)/C_0$, where $C_s\left(\bar{x},\bar{y},\bar{t}\right)$ [M L^{-3}] is the solute mass per unit volume of interstitial fluid (i.e., as opposed to per bulk sediment volume) and $\bar{\tau}\left(\bar{x},\bar{y}\right) = \tau\left(\bar{x},\bar{y}\right)/t_{\mathrm{T}}$ is a dimensionless form of the location-dependent residence time function, $\tau\left(\bar{x},\bar{y}\right)$ [T], defined as the time it takes interstitial water parcels to travel from the SWI to any

$(\bar{x},\bar{y})$ position in the sediment bed (Azizian et al., 2015) (derivation in Supplemental Information, **Text S3**):

$$\bar{\tau}(\bar{x},\bar{y})=\frac{\cos^{-1}\left[\cos\bar{x}e^{-\bar{y}}\right]-\bar{x}}{2\cos\bar{x}e^{-\bar{y}}},\ \bar{y}>0,\ -\pi/2<\bar{x}<\pi/2 \tag{8a}$$

The unsteady solution for the interstitial concentration of a conservative solute in the streambed directly follows from this last result, where the time-dependent solute concentration in the water column, $\bar{C}_w(\bar{t})$, is given by equation (5a):

$$\bar{C}_s(\bar{x},\bar{y},\bar{t})=\begin{cases}\bar{C}_w\left(\bar{t}-\bar{\tau}(\bar{x},\bar{y})\right),\ \bar{t}\geq\bar{\tau}(\bar{x},\bar{y})\\ 0,\ \bar{t}<\bar{\tau}(\bar{x},\bar{y})\end{cases},\ \bar{t}>0,\ \bar{y}>0 \tag{8b}$$

It should be noted that equation (8a) is valid only within the bounds of the unit cell illustrated in **Figure 1c** (i.e., $-\pi/2<\bar{x}<\pi/2$). Outside of the unit cell the equation must be translated, with or without reflection, using the following substitution rule for the dimensionless horizontal coordinate: $\bar{x}\rightarrow(-1)^n(\bar{x}-n\pi)$, where the integer n is given by $n=\mathrm{R}[\bar{x}/\pi]$ and the function $\mathrm{R}[\bullet]$ rounds to the nearest positive or negative integer value. Finally, a solution for the location of the concentration front in the sediment bed at any dimensionless time $\bar{t}$ can be obtained by substituting $\bar{t}$ for $\bar{\tau}$ on the left hand side of equation (8a), and numerically solving the resulting implicit expression for $\bar{y}$ given $\bar{x}$, or vice versa. The implicit solution for the concentration front also applies to locations outside of the unit cell (i.e., for $\bar{x}<-\pi/2$ or $\bar{x}>\pi/2$) after translation with or without reflection, using the substitution rule presented above for $\bar{x}$.

3. Diffusive Model of Hyporheic Exchange by Bedform Pumping

280 Advective models, like the BPM, are premised on the idea that pore-scale advection dominates
281 the transport of solutes in the hyporheic zone. Over the years, researchers have also explored the
282 possibility of employing diffusive models to describe hyporheic exchange, generally, and
283 bedform pumping, in particular (O'Connor and Harvey (2008)). EB, for example, argued that a
284 diffusivity for bedform pumping should take the form of a dispersion coefficient, $E \approx 0.04 \lambda u_m / \theta$
285 [L^2 T^{-1}], where u_m / θ is a characteristic pore-scale velocity associated with the BPM (see
286 equation (R5) in **Figure 1**)) and the mixing length-scale is the bedform wavelength, λ (from
287 equation (11) in Elliott and Brooks (1997b)). Applied to mass transfer in recirculating flumes,
288 the constant diffusivity model predicts that the water column solute concentration, and the
289 penetration depth of solute into the streambed, should both scale with the square root of time
290 (Elliott and Brooks (1997a,b)). In their recirculating flume experiments, EB found that mass
291 transfer across the SWI followed the predicted square root dependence until a transition time of
292 around, $t_c \approx 8 \lambda \theta / u_m$. Afterwards, measured mass transfer rates fell below those predicted by the
293 constant diffusivity model. Similarly, Marion and Zaramella (2005) reported that constant
294 diffusivities inferred from recirculating flume studies decline as the timescale over which
295 hyporheic exchange is measured increases.

296 From a mechanistic perspective, all of these problems with the constant diffusivity model
297 can be rationalized by noting that, as time increases, mass transfer across the SWI slows
298 dramatically as the relative contribution of deeper streamlines to bedform pumping increases
299 (i.e., streamlines with starting positions in the range, $\bar{x}_{0c} < \bar{x}_0 < \pi/2$, **see Section 1** of SI). We
300 hypothesize that this effect can be represented by requiring the dispersion coefficient to decline
301 exponentially with depth, in keeping with the exponentially declining velocity field that
302 underpins hyporheic exchange by bedform pumping (see equations (R2) - (R4) in **Figure 1**).

3.1. Governing Equations for Diffusive Bedform Pumping in a Closed System

Bedform pumping generates concentration fields in the interstitial fluids of the sediment bed that are at least two-dimensional (e.g., for artificially shaped triangular bedforms in the laboratory) and more often three-dimensional (e.g., in natural streams). However, if the goal is to predict average rates of mass transfer over, for example, a stream reach or a recirculating flume, knowledge of the two- and three-dimensional flow and subsurface concentration fields are not required. Thus, for many applications, mass transport and mixing by bedform pumping in the benthic biolayer can be conceptualized as an unsteady one-dimensional diffusion problem, for which the horizontally averaged vertical flux, $J(y,t)$ [M L^{-2} T^{-1}], of solute through the sediment is described by a flux-gradient diffusive model where the mixing coefficient, or effective diffusivity $D_{\text{eff}}(y)$ [L^2 T^{-1}], varies with depth through the benthic biolayer:

$$J(y,t) = -D_{\text{eff}}(y)\frac{\partial(\theta C_s)}{\partial y} \tag{9a}$$

Grant et al. (in review) demonstrated that equation (9a) is a reasonable descriptor of vertical solute transport by turbulent pumping through the benthic biolayer of a flat streambed, provided that the diffusion coefficient declines exponentially through the sediment bed. In this paper we hypothesize that a similar result applies to bedform pumping, but with the effective diffusivity replaced by an exponentially declining dispersion coefficient, $D_{\text{eff}}(y) = E(y) = E_0 e^{-ay}$. The surficial dispersion coefficient at the SWI, E_0 [L^2 T^{-1}], and the inverse decay length-scale, a [L^{-1}], are emergent properties of the two and three dimensional flow and concentration fields that drive bedform pumping; i.e., they are determined by spatial correlations between the time-averaged vertical component of the velocity field and the local mean solute concentration (Voermans et al., 2017). The corresponding one-dimensional mass balance equation can be written as follows:

$$\frac{\partial}{\partial t}\left(\theta C_s\right)=\frac{\partial}{\partial y}\left(E\left(y\right)\frac{\partial\left(\theta C_s\right)}{\partial y}\right) \tag{9b}$$

Equation (9b) equates the accumulation of mass in a differential horizontal slice of the sediment bed (left hand side) to the vertical diffusive transport (right hand side) of a conservative (non-reactive and non-adsorbing) solute (Incropera et al., 2007). The coordinate y increases with depth into the streambed and its origin (at $y=0$) is positioned at the horizontal plane of the SWI (**Figure 1b**).

Substituting the proposed functional form for the dispersion coefficient into equation (9b and assuming streambed porosity θ does not vary substantially over the vertical dimension of the benthic biolayer (*ca*., 5 cm) (Knapp et al., 2017), we arrive at the following mass balance equation for interstitial solute transport in the sediment bed:

$$\frac{\partial\overline{C}_s}{\partial\overline{t}}=e^{-\overline{y}}\frac{\partial^2\overline{C}_s}{\partial\overline{y}^2}-e^{-\overline{y}}\frac{\partial\overline{C}_s}{\partial\overline{y}},\ \overline{y}>0,\ \overline{t}>0 \tag{9c}$$

In equation (9c), time, $\overline{t}=t/t_{\mathrm{E}}$, has been scaled by a characteristic timescale for dispersive mass transport through the benthic biolayer, $t_{\mathrm{E}}=1/\left(a^2E_0\right)$, depth has been scaled by the inverse mixing length-scale, $\overline{y}=ay$, and the interstitial solute concentration has been scaled by the initial concentration in the overlying water column, $\overline{C}_s=C_s/C_0$ (same as for the BPM, see **Section 2.3**). By analogy to the BPM, we also assume that the streambed is initially solute free (equation (9d)), solute concentration drops off to zero deep in the streambed (equation (9e)), and the interstitial solute concentration at the top of the streambed equals the solute concentration in the overlying water column (equation (9f)) where $H\left(\overline{t}\right)$ [-] is the Heaviside function (included here to satisfy the requirements of Duhamel's Theorem described later):

$$\bar{C}_s\left(\bar{y},\bar{t}=0\right)=0 \tag{9d}$$

$$\bar{C}_s\left(\bar{y}\to\infty,\bar{t}\right)=0 \tag{9e}$$

$$\bar{C}_s\left(\bar{y}=0,\bar{t}\right)=\bar{C}_w\left(\bar{t}\right)H\left(\bar{t}\right),\ H\left(\bar{t}\right)=\begin{cases}0,\ \bar{t}<0\\1,\ \bar{t}>0\end{cases} \tag{9f}$$

In writing equation (9f) we have assumed that the interstitial concentration at the SWI is equal to the solute concentration in the overlying water column, which implies that mass transfer into the streambed is not rate-limited by convective mass transfer across the concentration boundary layer above the streambed; i.e., the dimensionless Biot Number—the ratio of timescales for diffusive mixing in the streambed and convective mass transfer across the turbulent boundary layer above the streambed—is much greater than unity (Incropera et al., 2007).

For a closed system with a well-mixed water column, like the recirculating flume illustrated in **Figure 3a**, mass balance over the water column takes the following form:

$$A_b h_w \frac{dC_w}{dt}=A_b\theta E_0\left.\frac{\partial C_s}{\partial y}\right|_{y=0,t} \tag{10a}$$

In this equation, the change of solute mass in the overlying water column and recirculation system of the flume (left hand side) equals the mass transfer rate across the SWI by bedform pumping (represented here as a dispersive process, right hand side). Streambed porosity θ appears on the right-hand side of the equation to account for the abrupt change in area over which solute mass transport occurs above and below the SWI (Grant et al., 2012). Expressing equation (10a) using the dimensionless variables introduced above for the diffusion equation, we obtain equation (10b) where $\bar{h}_w$ is a scaled form of the effective water depth.

$$\frac{d\bar{C}_w}{d\bar{t}}=\frac{1}{\bar{h}_w}\left.\frac{\partial\bar{C}_s}{\partial\bar{y}}\right|_{\bar{y}=0,\bar{t}} \tag{10b}$$

$$\bar{h}_w = \frac{a h_w}{\theta} \tag{10c}$$

3.2. Duhamel's Theorem and Green's Functions

As detailed in Grant et al. (in review), we can link the mass balance equations above (equation (10b)) and below (equation (9c)) the SWI, and thereby account for two-way coupling across the SWI, using Duhamel's Theorem, an analytical approach for solving the diffusion equation in cases where the forcing function at one boundary is a piece-wise continuous function of time (Perez Guerrero et al., 2013). Duhamel's Theorem allows us to express the evolution of interstitial solute concentration in the sediment bed as a convolution of the water column concentration $C_w(\bar{t})$ and a so-called auxiliary function $C_s^A(\bar{y},\bar{t})$ where v is a dummy integration variable (Perez-Guerrero et al., 2013):

$$\bar{C}_s(\bar{y},\bar{t}) = \int_0^{\bar{t}} \bar{C}_s^A(\bar{y},\bar{t}-v)\frac{d}{dv}\left[\bar{C}_w(v)U(v)\right]dv \tag{11a}$$

The auxiliary function is a solution to the same system of equations (equations (9c), (9d), (9e), and (9f)), but with the inhomogeneous term replaced by a unit step function (compare equations (9f) and (11e)):

$$\frac{\partial \bar{C}_s^A}{\partial \bar{t}} = e^{-\bar{y}}\frac{\partial^2 \bar{C}_s^A}{\partial \bar{y}^2} - e^{-\bar{y}}\frac{\partial \bar{C}_s^A}{\partial \bar{y}} \tag{11b}$$

$$C_s^A(\bar{y},\bar{t}=0) = 0,\ \bar{y} \geq 0 \tag{11c}$$

$$C_s^A(\bar{y}\to\infty,\bar{t}) = 0 \tag{11d}$$

$$C_s^A(\bar{y}=0,\bar{t}) = H(\bar{t}) \tag{11e}$$

Substituting the coordinate transformation, $\xi = e^{\bar{y}}$, into equation (11b) (Yates, 1992) and solving the resulting system of equations in the Laplace Domain, we arrive at the following analytical

385 solution for the auxiliary function where $\overline{s} = s t_E$ is a dimensionless form of the Laplace

386 Transform variable:

387 $$\tilde{C}_s^U\left(\overline{y},\overline{s}\right) = \frac{\sqrt{e^{\overline{y}}}}{\overline{s}} \frac{K_1\left(2\sqrt{\overline{s}e^{\overline{y}}}\right)}{K_1\left(2\sqrt{\overline{s}}\right)} \quad (12)$$

388 Duhamel's Theorem (equation (11a)) can also be expressed as a convolution of the

389 dimensionless water column concentration, $\overline{C}_w\left(\overline{t}\right)$, and a so-called Green's function, $G\left(\overline{y},\overline{t}\right)$ [T^{-1}],

390 which is scaled here by the dispersive mixing timescale introduced earlier, $\overline{G}\left(\overline{y},\overline{t}\right) = t_E G\left(\overline{y},\overline{t}\right)$:

391 $$\overline{C}_s\left(\overline{y},\overline{t}\right) = \int_0^{\overline{t}} \overline{G}\left(\overline{y},\overline{\tau}\right)\overline{C}_w\left(\overline{t}-\overline{\tau}\right)d\overline{\tau} \quad (13a)$$

392 $$\overline{G}\left(\overline{y},\overline{t}\right) = \frac{\partial \overline{C}_s^U}{\partial \overline{t}} \quad (13b)$$

393 Substituting equation (12) into equation (13b) yields a Green's function for the exponentially

394 declining diffusivity profile:

395 $$\overline{G}_E\left(\overline{y},\overline{t}\right) = \sqrt{e^{\overline{y}}}\,\mathcal{L}^{-1}\left[\frac{K_1\left(2\sqrt{\overline{s}e^{\overline{y}}}\right)}{K_1\left(2\sqrt{\overline{s}}\right)}\right] \quad (13c)$$

396 The similarity between equation (13a) and the convolution integral derived earlier for the BPM

397 (equation (1a)) is striking. In both cases, the water column concentration is convolved with a

398 function (Green's function in the case of the diffusive model and an RTD function in the case of

399 the advective model) that captures the response of the streambed to an impulsive injection of

400 mass into the SWI at dimensionless time $\overline{t} = 0$, $\overline{C}_w\left(\overline{t}\right) = \delta\left(\overline{t}\right)$, where $\delta\left(\overline{t}\right)$ [-] is the Dirac Delta.

401 The Green's function above (equation (13c)) is specific for the choice of an exponentially

402 decaying diffusivity profile. For the same set of initial and boundary conditions, a second

403 Green's function can be derived for a constant diffusivity profile (the so-called "Signaling

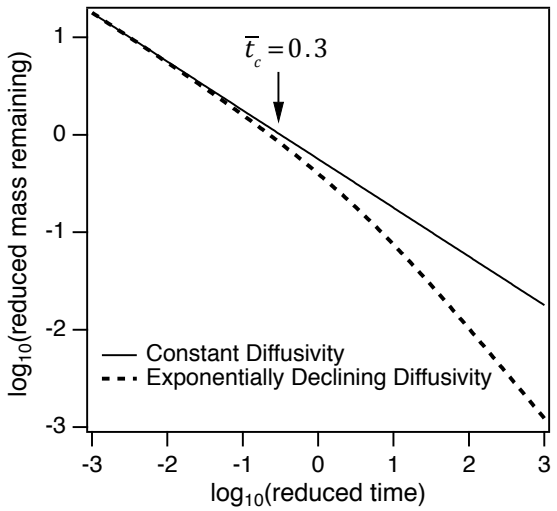

Figure 4. Scaling behavior for mass remaining in the streambed after an impulsive injection of mass at the SWI at time $\overline{t}=0$. Green's function predictions for the constant diffusivity and exponentially declining diffusivity models are shown.

Problem", see Gorenflo and Mainardi, 1988): $\overline{G}_{\mathrm{C}}\left(\overline{y},\overline{t}\right)=\overline{y}e^{-\overline{y}^2/\left(4\overline{t}\right)}\Big/\left(2\overline{t}\sqrt{\pi\overline{t}}\right)$. With these two Green's functions we can interrogate how the choice of a diffusivity profile (i.e., exponentially declining or constant) influences the temporal scaling of mass remaining in the sediment bed following an impulsive input of mass at the SWI at time $\overline{t}=0$. This is because, for $\overline{t}>0$, the upper boundary condition for these two Green's functions is zero, $\overline{C}_w\left(\overline{t}>0\right)=\delta\left(\overline{t}>0\right)=0$, and therefore solute mass in the sediment bed, $\overline{m}=\int_0^\infty \overline{G}\left(\overline{y},\overline{t}\right)d\overline{y}$,

will diffuse back into the water column after its injection at time $\overline{t}=0$:

$$\overline{m}_{\mathrm{E}}\left(\overline{t}\right)=\mathcal{L}^{-1}\left[\frac{K_0\left(2\sqrt{s}\right)}{\sqrt{s}K_1\left(2\sqrt{s}\right)}\right] \tag{14a}$$

$$\overline{m}_{\mathrm{C}}\left(\overline{t}\right)=\frac{1}{\sqrt{\pi\overline{t}}} \tag{14b}$$

As might be expected based on the discussion at the beginning of **Section 3**, the constant diffusivity model predicts solute mass remaining in the sediment bed declines inversely with the square root of time (equation (14b)). The exponentially declining diffusivity model (equation (14a)) exhibits this same $1/\sqrt{\overline{t}}$ scaling initially, but falls off more rapidly after $\overline{t}_c=t_c/t_E\approx 0.3$

(**Figure 4**). This result can be rationalized by noting that, for an exponentially declining diffusivity profile, deeper portions of the streambed are relatively inaccessible to solute injected at the SWI at $\bar{t}=0$ and consequently contribute little to the release of stored mass at long times. The similarity between the scaling behavior illustrated in **Figure 4** and the scaling behavior described earlier for mass transfer across the SWI in recirculating flumes (see preamble to **Section 3**) is the first indication that our overarching hypothesis—that bedform pumping can be represented by an exponentially decaying diffusivity model—may be valid.

3.3. Solute Concentration in the Water and Sediment Columns of Closed System

From the results presented above, a set of explicit solutions can be derived for solute concentration in the water column and interstitial fluids of a closed system (Grant et al., in review):

$$\bar{C}_w\left(\bar{t}\right)=\mathcal{L}^{-1}\left[\frac{1/\bar{s}}{1-\frac{1}{\bar{s}\bar{h}_w}\left(\partial\tilde{G}/\partial\bar{y}\right)_{\bar{y}=0,\bar{s}}}\right] \tag{15a}$$

$$\bar{C}_s\left(\bar{y},\bar{t}\right)=\mathcal{L}^{-1}\left[\frac{\tilde{G}\left(\bar{y},\bar{s}\right)/\bar{s}}{1-\frac{1}{\bar{s}\bar{h}_w}\left(\partial\tilde{G}/\partial\bar{y}\right)_{\bar{y}=0,\bar{s}}}\right] \tag{15b}$$

These analytical solutions are written in terms of the Laplace transform of the Green's function and its derivative, which, in this context, are tailored to the choice of diffusivity profile. For an exponentially declining diffusivity profile, they are as follows:

$$\tilde{G}_{\mathrm{E}}\left(\bar{y},\bar{s}\right)=\sqrt{e^{\bar{y}}}\frac{K_1\left(2\sqrt{\bar{s}e^{\bar{y}}}\right)}{K_1\left(2\sqrt{\bar{s}}\right)} \tag{15c}$$

$$\left.\frac{\partial\tilde{G}_{\mathrm{E}}}{\partial\bar{y}}\right|_{\bar{y}=0,\bar{s}}=-\frac{\sqrt{\bar{s}}K_0\left(2\sqrt{\bar{s}}\right)}{K_1\left(2\sqrt{\bar{s}}\right)} \tag{15d}$$

For a constant diffusivity profile, these two functions can be computed directly from the solution to the Signaling Problem introduced earlier:

$$\tilde{G}_C\left(\bar{y},\bar{s}\right)=e^{-\bar{y}\sqrt{\bar{s}}} \tag{15e}$$

$$\left.\frac{\partial\tilde{G}_C}{\partial\bar{y}}\right|_{\bar{y}=0,\bar{s}}=-\sqrt{\bar{s}} \tag{15f}$$

4. Experimental Evaluation of Advective and Diffusion Models of Bedform Pumping

4.1. EB's Bedform Pumping Dataset and Model Optimization

To test the parallel advective and diffusive analytical frameworks derived above, we turned to one of the first published recirculating flume experiments specifically designed, along the lines of **Figure 3a**, to investigate the unsteady transfer of a conservative solute across the SWI by bedform pumping (Elliott and Brooks, 1997b). EB's experiments were conducted with stationary bedforms (either artificial triangular bedforms or natural ripples), a non-adsorbing and stable fluorescent dye (Lissamine), and under various flow velocities (8.6 to 13.2 cm s^{-1}), water depths (1.14 to 2.54 cm) and shear velocities (1.3 to 3 cm s^{-1}) (Experiment ID's 8, 9, 12, 14 – 17). The sediment bed, which ranged in depth from 12.5 to 22.0 cm depending on the experiment, consisted of medium or fine-grained unconsolidated sand of hydraulic conductivity $K_h =$ 0.11 and 0.0079 cm s^{-1} and porosity $\theta =$ 0.325 and 0.295, respectively (a summary of experimental conditions is included in the Supplemental Information, **Table S1**). Published over 20 years ago, EB's study remains one of the few where the evolution of dye concentration is followed both above and below the SWI—a feature we will take advantage of here.

Experimental evaluation of our analytical models was carried out in two steps. First, we fit the advective and diffusive models for $C_w\left(t\right)$ (equations (5a) and (15a), respectively) to EB's

463 measurements of dye concentration in the water column over time. This was accomplished using
464 the NonLinearModelFit routine in the Mathematica computing package (v.12, Wolfram
465 Research, Inc.) implemented on UC Irvine's High-Performance Computing Cluster. Laplace
466 inversions were carried out by Gaussian Quadrature in the Mathematica package authored by U.
467 Graf (Graf, 2004). This fitting exercise yielded, for each of EB's experiments, inferred values for
468 the half-amplitude of the pressure head variation and effective water depth (h_m and h_w, advective
469 model) and the surficial dispersion coefficient and inverse mixing length-scale (E_0 and a,
470 diffusive model), together with the standard deviation of each parameter and the model's
471 coefficient of variation (R^2). For consistency, h_w values inferred from the advective model were
472 applied to the diffusive model; all other parameters (θ, K_h, λ, and C_0) were reported by EB for
473 each experiment (see **Table S1**). In the second step, parameter values inferred from the water
474 column studies were used to predict the movement of dye through the interstitial fluids of the
475 streambed over time (equations (8b) and (15b)). These model predictions were compared to
476 observations of the dye front in the sediment bed, which EB recorded by periodically marking
477 the location of the leading edge of the dye plume on the side of their flume (the wall of the flume
478 was transparent, and dye was visualized with a hand-held UV light).

479 **4.2. Evaluation of Model-Predicted Water Column Solute Concentrations**

480 Across all seven experiments, the advective model (equation (5a)) and diffusive model (with an
481 exponentially declining diffusivity profile, equation (15a)) closely conform to EB's time series
482 measurements of dye concentration in the water column ($R^2 >$ 0.9998 for both models, **Figure**
483 **5a,b**, also see **Tables S2** and **S3** in the Supplemental Information). For comparison, water
484 column concentrations for Experiment #17 were also simulated with the constant diffusivity
485 model; this involved substituting equation (15f) into equation (15a) and adopting the superficial

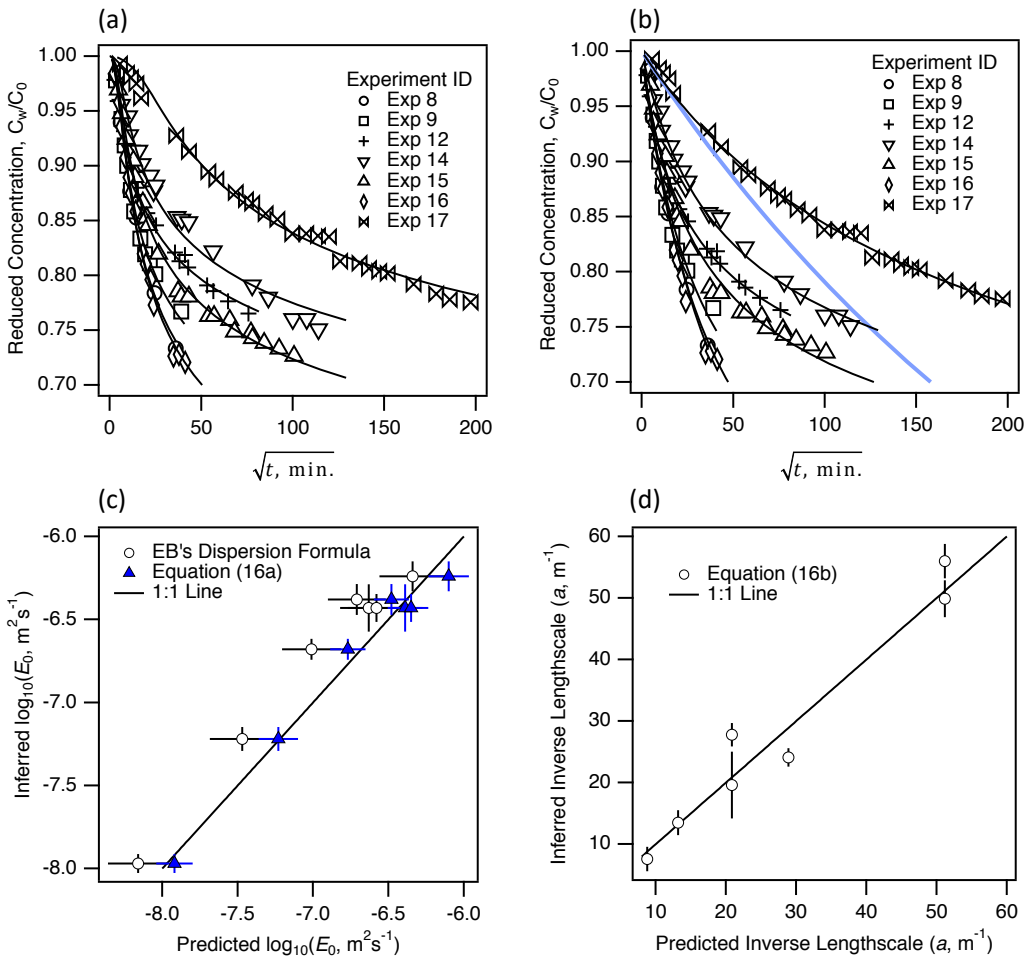

Figure 5. Advective (**a**) and diffusive (**b**) models of bedform pumping (solid black curves) conform equally well to EB's measurements of dye concentration over time (symbols), provided that the diffusive model's dispersion coefficient decays exponentially with depth. For comparison, the constant diffusivity model's prediction for Experiment #17 is shown (blue curve). (**c**) Surficial diffusivities inferred from the diffusive model (vertical axis) correlate strongly with surficial diffusivities estimated by substituting values of h_m inferred from the advective model into EB's dispersion coefficient formula before (open circles) or after (blue triangles, equation (16a)) bias correction. (**d**) Inverse decay length scales inferred from the diffusive model (vertical axis) correlate strongly with the inverse of the average bedform wavelength (bottom axis, equation (16b).

diffusivity, E_0, inferred from fitting the exponentially declining diffusivity model to the same dataset (**Table S3**). The constant diffusivity model also conforms to measurements of the water

488 column concentration until around $\sqrt{t} \approx \sqrt{30}$ min$^{1/2}$; thereafter, the constant diffusivity model
489 seriously underpredicts observed concentration measurements (blue curve, **Figure 5b**). Water
490 column concentrations predicted by the constant diffusivity model decline approximately linearly
491 when plotted against $\sqrt{t}$, consistent with EB's observations about the constant diffusivity model
492 (see preamble to **Section 3**) and the $\sqrt{t}$-scaling of the constant diffusivity's Green's function
493 (see equation (14b) and **Figure 4**).

494 We can also evaluate the advective and diffusive models based on how well their inferred
495 parameter values reproduce values expected based on theory or measurements. For example,
496 values of the half-amplitude pressure head inferred from the advective model (ranging from h_m =
497 0.04 to 0.57 mm) are similar (roughly factor of two or better) to values estimated from EB's
498 empirical formula (equation (7)) (ranging from h_m = 0.09 to 0.31 mm, **Table S2**). Likewise,
499 values of the effective water depth inferred from the advective model (ranging from h_w = 8.8 to
500 16.7 cm) are similar (roughly factor of two or better) to values estimated from reported flume
501 water volume (excluding interstitial fluid) and streambed area ($h_w = V_w / A_b$ = 11.3 to 12.5 cm)
502 (**Table S2**). Deviations between inferred and predicted (or measured) values of h_m and h_w do not
503 necessarily imply that the model-generated values are incorrect. For example, the half-amplitude
504 head values predicted by equation (7) are only approximately correct (Shen et al., 1990; Fox et
505 al., 2014). Measurement errors associated with flume water volume and bed surface area (which
506 may be difficult to define, given the undulatory nature of the SWI with bedforms) also contribute
507 uncertainty and bias to experimental estimates of h_w.

508 A more rigorous assessment of the inferred parameter values can be framed as follows:
509 *Can parameter values inferred from the advective model be translated directly into parameter*

values for the diffusion model and vice versa? To answer this question, we equated EB's proposed formula for a bedform pumping dispersion coefficient to the diffusivity model's surficial dispersion coefficient: $E_0 \approx 0.04 \lambda u_m / \theta$. Substituting the BPM's solution for the maximum Darcy flux (u_m, equation (R5) in **Figure 1**), this formula predicts that the diffusive model's surficial dispersion coefficient is directly proportional to the advective model's half-amplitude pressure head, $E_0 \approx 0.08 \pi K_h h_m / \theta$. When values of h_m inferred from the advective model are substituted into this formula, the predicted values of E_0 are highly correlated with values of E_0 inferred from the diffusion model (Pearson's Correlation coefficient, $R = 0.99$) (open black circles, **Figure 5c**). Adjusting the equation's pre-factor to correct the bias evident in the figure, we arrive at the following relationship between the advective and dispersive descriptions of bedform pumping (blue filled triangles, **Figure 5c**):

$$E_0 \approx 0.133 \pi K_h h_m / \theta, \quad 0.08 \leq K_h \left[mm s^{-1} \right] \leq 1.1, \; 0.042 \leq h_m \left[mm \right] \leq 0.11, \; 0.295 \leq \theta \leq 0.325 \qquad (16a)$$

Likewise, the inverse decay length-scale, a, inferred from the diffusion model is highly correlated ($R^2 = 0.95$) with the inverse of the average bedform wavelength (**Figure 5d**):

$$a \left[cm^{-1} \right] = 5.28 / \lambda \left[cm \right] - 0.0882, \quad 8.8 \leq \lambda \left[cm \right] \leq 30 \qquad (16b)$$

Equations (16a) and (16b) provide a direct link between our advective and diffusive descriptions of bedform pumping, such that a parameter set for one can be directly translated into a parameter set for the other. The implication is that these two descriptions of bedform pumping are, in fact, functionally equivalent, provided that the limitations with existing analytical models outlined earlier (water column concentration constant in time, diffusivity is constant in depth, two-way coupling across the SWI neglected, and the sediment bed's finite porosity neglected) are properly addressed, as they have been in this study. Because equations (16a) and (16b) are calibrated with

data from EB's study alone, they are per force restricted to a limited range of flow and streambed conditions (indicated by the inequalities above). A meta-analysis is underway to evaluate the predictive power of these equations beyond the set of experiments analyzed here.

4.3. Evaluation of Model-Predicted Interstitial Solute Concentrations

We can also evaluate the advective and diffusive models relative to their ability to predict the unsteady transport of dye plumes through the interstitial fluids of the sediment bed. The progression of one such plume beneath an artificial triangular ripple (EB's Experiment #9) is reproduced in **Figures 6a - d** (thick dashed curves). The dye plume penetrated to a depth of about 8 cm in the first 75 minutes, but required an additional 575 minutes to progress downward another 4 cm. To compare these observations with the advective model solution, the BPM's coordinate system must first be aligned with EB's triangular ripple. To this end we used the parameter values estimated from the water column optimization study of Experiment #9 (see **Table S2**) to predict (with equation (8b)) the interstitial dye concentration in the sediment bed at $t = 75$ minutes, coinciding with EB's first dye front measurement. The model's horizontal coordinate was adjusted to align the left and right edges of the observed and predicted dye fronts. Finally, the model's vertical coordinate was adjusted so that the top of the (flat) model domain is equidistant between the crest and trough of the triangular bedform (final alignment is shown in **Figure 6a**). After making these adjustments, the advective model's predictions for the downward migration of the dye plume over time closely agree with EB's observations of the dye front at $t =$ 150, 320, and 650 minutes (**Figures 6b - 6d**).

Two-way coupling is also evident in the model-predicted interstitial concentration field. Predicted dye concentrations are elevated along the front of the plume because water parcels at the front moved into the sediment bed near time $t = 0$ when dye concentration in the water

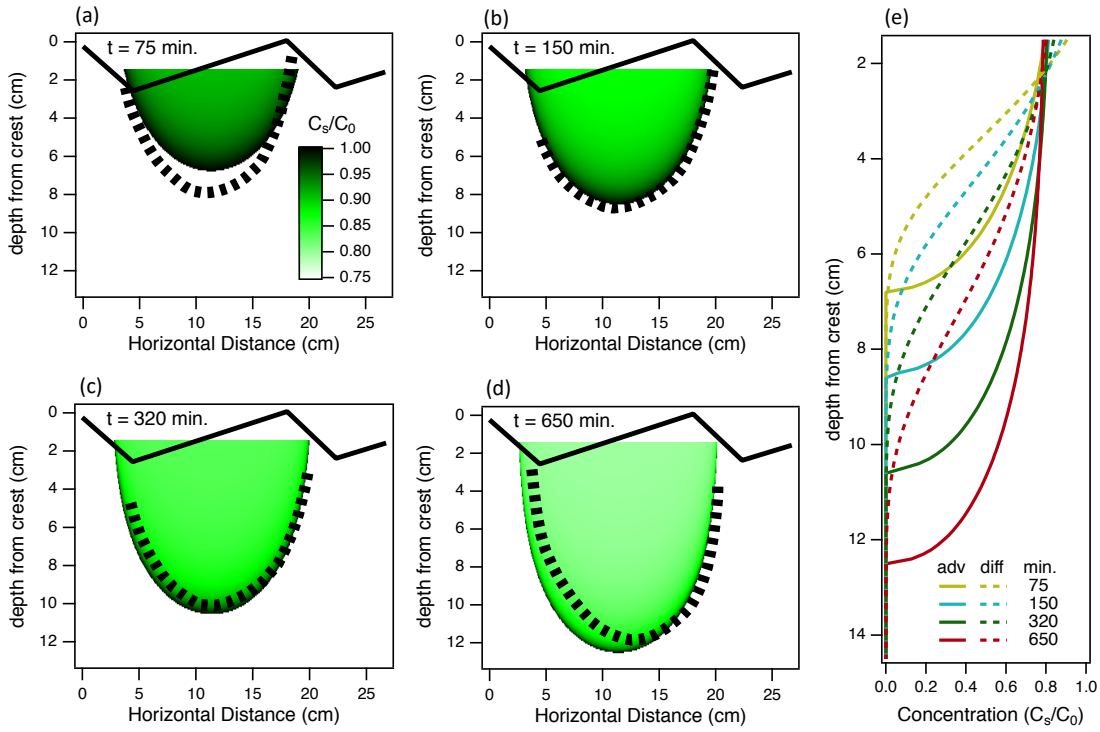

Figure 6 (**a**) – (**d**) The downward migration of a dye plume in the sediment bed beneath an artificial triangular ripple during EB's Experiment #9 (shape of the ripple indicated at the top of each panel). Thick black dashed curves denote the observed location of the dye front at the elapsed times indicated (adapted from Figure 2 of Elliott and Brooks (1997b)). Green color scale indicates the interstitial dye concentration predicted by equation (8b) after adjusting the model's vertical and horizontal coordinates (see text). (**e**) Dimensionless concentration depth profiles at the same elapsed times predicted by the diffusive model (dashed curves) and horizontally averaged advective model (solid curves).

column was near its initial (maximum) value, $C_w = C_0$. As time progresses, dye concentration in the water column declines and the trailing edge of the dye plume, which consists of younger water parcels, becomes less concentrated. This pattern—high dye concentration along the plume's front and low concentration along the plume's trailing edge—is particularly striking for the simulation at $t = 150$ (**Figure 6b**). Eventually the plume's concentration field takes on a

560 more uniform appearance as older water parcels (with higher dye concentrations) return to the
561 stream along slow moving streamlines (**Figure 6d**).

562 Thus far we have found little difference between our advective and diffusive models of
563 bedform pumping. One aspect where these two models differ substantially is their respective
564 concentration depth profiles (**Figure 6e**). The diffusivity model's depth profiles are convex in
565 shape and characterized by a diffuse concentration front that becomes increasingly smeared out
566 over the vertical extent of the streambed with increasing time. By contrast, the advective
567 concentration depth profiles (generated by horizontally averaging the two-dimensional
568 concentration fields appearing in **Figures 6a** – **6d**) are convex and characterized by persistent
569 and very sharp concentration fronts. These contrasting shapes, which reflect the purely advective
570 and diffusive transport mechanisms underlying the two modeling frameworks, could lead to very
571 different predictions for the transport of reactive solutes through the benthic biolayer. This begs
572 the question: *which of these two profiles is more representative of natural systems*?

573 To answer this question, we turned to recirculating flume experiments EB conducted
574 with stationary natural ripples. These experiments entailed operating the flume under high flow
575 conditions (to induce sediment transport and ripple formation) and then lowering the flow
576 velocity (to immobilize the bedforms and conduct the dye exchange experiments). Not
577 surprisingly, dye plumes generated by natural ripples are variable with respect to their horizontal
578 extent and the depth to which dye penetrates the streambed (**Figure 7a**). This variability, which
579 arises from variations in bedform geometry (i.e., height H and wavelength λ) and the three-
580 dimensional nature of natural ripples, can be formally analyzed using spectral methods (e.g.,
581 Stonedahl et al. (2010)). However, if the goal is to obtain bulk estimates for the downward

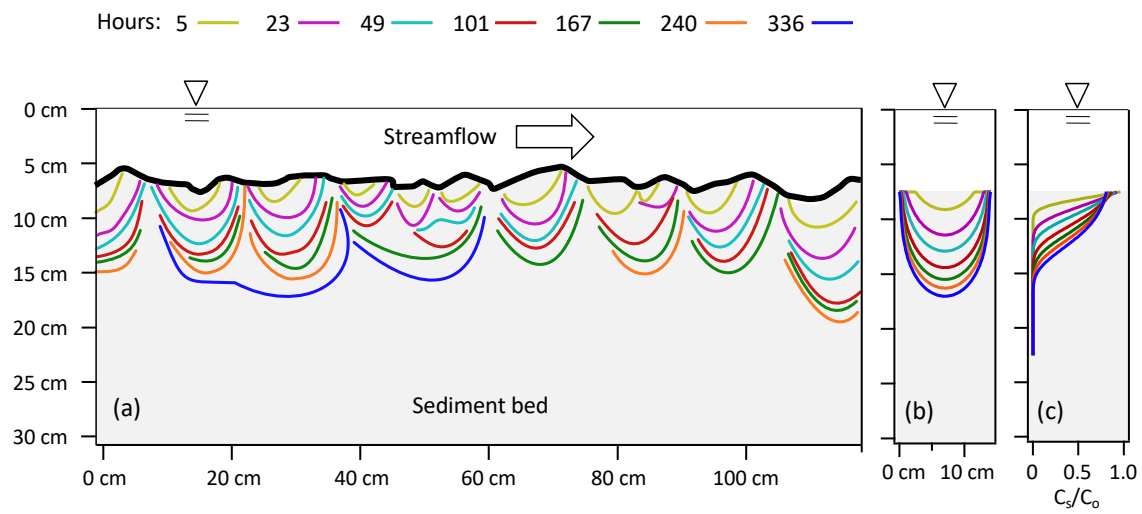

Figure 7. The downward movement of dye fronts in the sediment beneath natural ripples during EB's Experiment #17: (**a**) dye fronts observed at the various elapsed times indicated (adapted from Figure 3b of Elliott and Brooks (1997b)), (**b**) dye fronts predicted by the advective model of bedform pumping, (**c**) concentration depth profiles predicted by the diffusive model of bedform pumping. The depth of the sediment bed reflects actual experimental conditions for this experiment ($d_b = 22.5$ cm, see **Table S1**).

progression of solute through the benthic biolayer over time, both the advective and diffusive analytical solutions derived in this study perform remarkably well (compare **Figures 7a** – **7c**). The sharp dye fronts predicted by the advective model are comparable to patterns of dye penetration beneath "average" bedforms; e.g., the two dye plumes located 10 to 40 cm along the horizontal axis (**Figure 7a**). The smeared-out dye fronts predicted by the diffusive model, on the other hand, may be more representative of the concentration profile one would obtain by horizontally averaging the interstitial concentration field across all bedforms (this hypothesis could not be tested with EB's dataset because these authors recorded the time evolution of concentration fronts, not concentration fields). What these results imply for reactive solute transport through the benthic biolayer is an interesting topic for future study.

5. Discussion

593 The functional equivalence of the analytical advective and diffusive frameworks derived here
594 implies that their application can be tailored to the problem at hand. The advective model is a
595 relatively faithful representation of the two-dimensional interstitial flow fields associated with
596 bedform pumping. Consequently, this framework will be useful in cases where knowledge of
597 flow paths through the benthic biolayer, and their associated Darcy fluxes and residence times, is
598 required. The removal of stream borne particles in the benthic biolayer by deep bed filtration, for
599 example, requires detailed information about the interstitial flow field. This is because, as
600 particles move through the streambed, their filtration rate depends on the local flow velocity
601 (through the contact efficiency η_0 [-], see Tufenkji and Elimelech (2004)) which varies
602 continuously along a streamline (see equations (R1)-(R5) in **Figure 1**). Another example is the
603 spatial zonation of interstitial oxygen concentration beneath bedforms, including the formation of
604 so-called "anoxic chimneys" in upwelling zones (Kessler et al., 2012; Kessler et al., 2013;
605 Azizian et al., 2015). This biogeochemical zonation, which arises from the coupling between in-
606 bed redox reactions and bedform pumping of electron donors and acceptors, can impose
607 significant constraints on important streambed functions, such as coupled nitrification-
608 denitrification (Kessler et al., 2013). Because the advective model's flow field is quantitatively
609 linked to bedform geometry and stream flow (i.e., bedform height and wavelength, as well as
610 stream depth and velocity, see equation (7)), physicochemical (e.g., particle filtration) and
611 biogeochemical (e.g., nutrient transformation) functions of the benthic biolayer can be tied
612 directly to geomorphic processes, such as the adjustment of bedform morphology to changes in
613 land use and flow regime, for example as a result of urbanization (Harvey et al., 2012).
614 On the other hand, a strength of the diffusive model is its ability to combine multiple
615 mechanisms for mass transport across the SWI. As noted earlier, mixing across a flat SWI can be

616 characterized by an effective diffusivity, D_{eff} , that incorporates three transport mechanisms
617 (Richardson and Parr, 1988; O'Connor and Harvey, 2008; Grant et al., 2012; Voermans et al.,
618 2018): (1) tortuosity-modified molecular diffusion (D_{m} [L^2 T^{-1}]); (2) dispersion (D_{d} [L^2 T^{-1}]); and
619 (3) turbulent diffusion (D_{t} [L^2 T^{-1}]). The turbulent and dispersive diffusivities increase with the
620 Permeability Reynolds Number, $\mathrm{Re}_K = u_* \sqrt{K} / \upsilon$ [-], a dimensionless ratio of a permeability length
621 scale ($\sqrt{K}$ [L]) and the viscous length scale that governs turbulence at the surface of the
622 streambed (ratio of the kinematic viscosity of water υ [L^2 T^{-1}] and the shear velocity u_* [L T^{-1}])
623 (Voermans et al., 2017; Voermans et al., 2018). For turbulent mass transfer across a flat SWI, and
624 accounting for the exponential decay of diffusivity with depth, the surficial effective diffusivity
625 exhibits different Permeability Reynolds Number scaling behavior in the dispersive ($D_{\mathrm{eff},0} \propto \mathrm{Re}_K^{2.5}$,
626 $0.01 < \mathrm{Re}_K < 1$) and turbulent diffusive ($D_{\mathrm{eff},0} \propto \mathrm{Re}_K^{1}$, $\mathrm{Re}_K > 1$) regimes (Grant et al., in review). Our
627 formula linking advective and dispersive descriptions of bedform pumping (equation (16a))
628 implies that dispersive mixing by bedform pumping also increases with the Permeability
629 Reynold Number, $E_0 \propto \mathrm{Re}_K^2$. This last result can be demonstrated by substituting into equation
630 (16a) definitions for the Darcy-Weisbach friction factor, $f_{\mathrm{D}} = 8u_*^2 / V^2$ [-] (Sabersky and Acosta,
631 1989) and the streambed permeability, $K = \upsilon K_h / g$ [L^2] (McCabe et al., 2010), and noting that the
632 friction factor will likely scale with the fraction of the water depth taken up by a bedform,
633 $f_{\mathrm{D}} \propto \left(H/d \right)^{\gamma}$. Thus, the one-dimensional diffusive framework potentially solute mixing through the
634 benthic biolayer by molecular diffusion, turbulent dispersion, turbulent diffusion, and bedform
635 pumping.

Another advantage of the diffusive model is that it can be readily modified to account for groundwater recharge or discharge (through the addition of an advective term to equation (9a)) and the inclusion of biogeochemical reaction networks, such as the Monod kinetic expressions associated with nitrogen cycling in streambeds (respiration, ammonification, nitrification, and denitrification (Azizian et al., 2017)). While surface water-groundwater exchange can be factored into the BPM's flow field as well (c.f., Boano et al., 2008) doing so invalidates a key requirement of the advective model's predictions for solute transport; namely, that the x-component of the velocity is everywhere constant along a streamline (see **Text S1** in Supplemental Information). While outside of the scope of this paper, it is also interesting to note that, at sufficiently high celerity, bedform migration tends to reduce the complexity of the interstitial concentration fields, in effect transforming the complex two- and three-dimensional concentration fields associated with bedform pumping across stationary bedforms into simple one-dimensional vertical concentration gradients (e.g., of interstitial oxygen concentrations, Wolke et al., 2020) that may also be amenable to analysis with a diffusive modeling framework.

A benefit of analytical models (compared to numerical simulations) is the relative ease with which they can be implemented, and the physical insights afforded by expressing the quantity of interest (e.g., interstitial solute concentration or mass flux across the SWI) as an explicit function of key system variables. An obvious limitation is that their derivation often entails simplifying assumptions that may not be valid in practice. Key assumptions associated with the advective and diffusive modeling frameworks derived here include: (1) the interstitial flow field underlying bedform pumping is steady-state, although solute concentrations in the water column and interstitial fluids of the streambed may vary with time while fully accounting for two-way coupling across the SWI; (2) the solutions are specific to closed systems (such as

659 recirculating flumes) while most hyporheic exchange problems of practical interest are open
660 systems (such as streams and coastal sediments); (3) the transport properties of the benthic
661 biolayer (such as porosity and hydraulic conductivity) are assumed homogeneous and invariant
662 with time while a previous study found that these assumptions can be invalidated by bioclogging
663 (Caruso et al., 2017); and (4) as already noted, our results assume the solute in question is
664 conservative (i.e., non-reactive and does not absorb to the porous matrix) while most hyporheic
665 exchange problems of practical interest involve reactive solutes or particles. These limitations
666 can be addressed, to varying degrees, within the context of our analytical framework, and efforts
667 to do so are currently underway.

668 **6. Conclusions**

669 In this paper we derived two parallel analytical frameworks, one advective and the other
670 diffusive, that together relax many of the assumptions that limit the practical utility of presently
671 available analytical models for bedform pumping. Both frameworks allow the water column
672 concentration to vary with time while accounting for the two-way coupling of solute
673 concentrations above and below the SWI; the diffusive framework additionally allows the
674 mixing rate, or diffusivity, to vary with depth through the sediment bed. When applied to
675 previously published measurements of bedform pumping in a recirculating flume (Elliott and
676 Brooks, 1997a), we find that both analytical frameworks closely reproduce average patterns and
677 rates of hyporheic exchange, *provided that the diffusion model's diffusivity declines*
678 *exponentially with depth*. Practical application of these two frameworks can be tailored to the
679 problem at hand, depending on whether detailed knowledge of the interstitial flow fields and
680 associated Darcy fluxes and residence times is required (advective model) or solute transport
681 across the SWI is subject to multiple transport mechanisms, not just bedform pumping (diffusive
682 model). Because the advective framework is grounded in a physical description of bedform

683 pumping, it explicitly accounts for how changes in stream flow and sediment transport (e.g.,
684 associated with urbanization) influence bedform geometry (wavelength and height), the half-
685 amplitude of the pressure head variation, and the hydraulic conductivity of the sediment bed. The
686 exponentially declining diffusivity framework, on the hand, lumps these geomorphic processes
687 into a surficial dispersion coefficient and an inverse decay length-scale that can be directly
688 calculated from the aforementioned advective model parameters (see equation (16a,b)). The
689 latter formula also predicts that the surficial dispersion coefficient for bedform pumping
690 increases with the dimensionless Permeability Reynolds Number, consistent with diffusivities
691 measured for turbulent exchange across flat streambeds (Voermans et al., 2018; Grant et al., in
692 review) and streambeds with bedforms (O'Connor and Harvey, 2008; Grant et al., 2012; Grant et
693 al., 2018). Efforts are currently underway to extend these analytical solutions to open systems
694 (e.g., stream networks), bedform turnover, unsteady flows, and the non-linear reactions that drive
695 nutrient cycling in the benthic biolayer of streams.

696 **Acknowledgments and Data**

697 The authors declare no conflicts of interest. Data is available through Elliott and Brooks (1997b).
698 SBG was supported by the U.S. National Science Foundation (award 1840504), Virginia Tech's
699 ICTAS EFO Opportunity Seed Investment Grant, and the UC Office of the President Multi-
700 campus Research Program Initiative award (MRP-17-455083). AM was funded by Compagnia di
701 San Paolo through the 2017 call "Joint research project with top universities" (RINSE project).
702 JGV was funded by the U.S. National Science Foundation (award EAR 1830172) and the U.S.
703 Department of Energy, Office of Biological and Environmental Research (BER), as part of
704 BER's Subsurface Biogeochemistry Research Program (SBR). This contribution originates from
705 the SBR Scientific Focus Area (SFA) at the Pacific Northwest National Laboratory (PNNL). IG

was supported by UK EPSRC Established Career Fellowship (award EP/P012027/1). MG was funded by the Australian Research Council's Discovery Projects funding scheme (DP120102500). JH was supported by the USGS Water Resources Availability Program. SBG derived the models and drafted the paper; AM, FB, JDGV, IG, JH and MG edited the manuscript, assisted with the interpretation of results, and contributed text. The authors thank E. Gee and L. Grant for assistant with Figures 1 and 7, respectively, and M. Rippy for helpful edits.

References.

Azizian, M., Grant, S.B., Kessler, A.J., Cook, P.L.M., Rippy, M.A., Stewardson, M.J. (2015) Bedforms as biocatalytic filters: A pumping and streamline segregation model for nitrate removal in permeable sediments. *Environmental Science and Technology*, 49, 10993-11002.

Azizian, M., Boano, F., Cook, P.L.M., Detwiler, R.L., Rippy, M.A., & Grant, S.B. (2017), Ambient groundwater flow diminishes nitrate processing in the hyporheic zone of streams, *Water Resources Research*, 53, doi:10.1002/2016WR020048.

Boano, F., Revelli, R., Ridolfi, L. (2008), Reduction of the Hyporheic Zone Volume due to the Stream-Aquifer Interaction. *Geophysical Research Letters*, 35, L09401.

Boano, F., Harvey, J. W., Marion, A., Packman, A. I., Revelli, R., Ridolfi, L., & Wörman, A. (2014), Hyporheic flow and transport processes: Mechanisms, models, and biogeochemical implications. *Reviews of Geophysics*, 52, 603-679. https//doi:10.1002/2012RG000417

Bottacin-Busolin, A., and A. Marion (2010), Combined role of advective pumping and mechanical dispersion on time scales of bed form–induced hyporheic exchange, *Water Resources Research*, 46, W08518, doi:10.1029/2009WR008892.

Cardenas M.B. and Wilson (2007a), Hydrodynamics of coupled flow above and below a sediment–water interface with triangular bedforms, Advances in Water Resources, 30(3), 301-313, doi:10.1016/j.advwatres.2006.06.009

Cardenas, M.B. & Wilson, J.L. (2007b) Dunes, turbulent eddies, and interfacial exchange with permeable sediments. *Water Resources Research* 43, W08512.

Cardenas, M., J. L. Wilson, & R. Haggerty (2008), Residence time of bedform-driven hyporheic exchange. *Advances Water Research*, 31, 1382-1386.

Caruso, A., F. Boano, L. Ridolfi, D. L. Chopp, & A. Packman (2017), Biofilm-induced bioclogging produces sharp interfaces in hyporheic flow, redox conditions, and microbial community structure, *Geophys. Res. Lett*., 44, 4917–4925, doi:10.1002/2017GL073651.

Elliott, A. H., & N. H. Brooks (1997a), Transfer of nonsorbing solutes to a streambed with bed forms: Theory, *Water Resources Research*, 33, 123−136.

740 Elliott, A. H., & N. H. Brooks (1997b), Transfer of nonsorbing solutes to a streambed with bed
741 forms: Laboratory experiments. *Water Resources Research*, 33, 137−151.

742 Fehlman, H.M. (1985) Resistance components and velocity distributions of open channel flows
743 over bedforms. M.S. thesis, Colo. State Univ., Fort Collins.

744 Fleckenstein, J.H., Krause, S., Hannah, D.M., Boano, F. (2010), Groundwater-surface water
745 interactions: New methods and models to improve understanding of processes and dynamics. *Adv.*
746 *Water Resources*, 33, 1291-1295.

747 Fox A., Boano F., Arnon S. (2014), Impact of losing and gaining streamflow conditions on
748 hyporheic exchange fluxes induced by dune-shaped bed forms, Water Resour. Res., 50(3), 1895-
749 1907, doi:10.1002/2013WR014668

750 Gomez-Velez, J. D., & Harvey, J. W. (2014), A hydrogeomorphic river network model predicts
751 where and why hyporheic exchange is important in large basins. *Geophysical Research Letters*,
752 2014GL061099. https//doi:10.1002/2014GL061099

753 Gomez-Velez, J. D., Harvey, J. W., Cardenas, M. B., & Kiel, B. (2015), Denitrification in the
754 Mississippi River network controlled by flow through river bedforms. *Nature Geoscience*, 8,
755 941-945. https// doi:10.1038/ngeo2567

756 Gorenflo, R., & Mainardi, F. (1998), Fractional Calculus and Stable Probability Distributions.
757 *Archives in Mechanics*, 50, 377-388.

758 Graff, U. (2004) "Applied Laplace Transforms and z-Transforms for Scientists and Engineers—
759 A Computational Approach using a Mathematica Package", New York, NY, Springer-Basal AG,
760 1st Ed.

761 Grant, S. B. Stewardson, M. J. & Marusic, I. (2012), Effective diffusivity and mass flux across
762 the sediment-water interface in streams. *Water Resources Research*, 48, W05548.
763 https//doi:10.1029/2011WR011148

764 Grant, S. B., Stolzenbach, K., Azizian, M., Stewardson, M. J., Boano, F., & Bardini, L. (2014),
765 First-Order Contaminant Removal in the Hyporheic Zone of Streams: Physical Insights from a
766 Simple Analytical Model. Environmental Science and Technology, 48, 11369-11378.
767 doi:10.1021/es501694k

768 Grant, S. B., Azizian, M., Cook, P., Boano, F. & Rippy, M. A. (2018a), Factoring stream
769 turbulence into global assessments of nitrogen pollution. Science, 359, 1266-1269.
770 https//doi:10.1126/science.aap8074

771 Grant, S.B. Gomez-Velez, J.D., & Ghisalberti, M. (2018b), Modeling the effects of turbulence
772 on hyporheic exchange and local-to-global nutrient processing in streams. *Water Resources*
773 *Research*, 54, https//doi:10.1029/2018WR023078.

774 Grant et al. (2020) Vertical Structure and Scaling of Turbulent Mixing in the Benthic Biolayer of
775 Stream and Coastal Sediments. *Water Resources Research*, revision in review.

776 Harvey, J.W., Drummond, J.D., Martin, R.L., McPhillips, L.E., Packman, A.I., Jerolmack, D.J.,
777 Stonedahl, S.H., Aubeneau, A.F., Sawyer, A.H., Larsen, L.G., Tobias, C.R. (2012),
778 Hydrogeomorphology of the hyporheic zone: Stream solute and fine particle interactions with a
779 dynamic streambed. *J. Geophysical Research: Biogeosciences*, 117, G00N11.

780 Harvey, J. W., Böhlke, J. K., Voytek, M. A., Scott, D., & Tobias, C. R. (2013), Hyporheic zone
781 denitrification: Controls on effective reaction depth and contribution to whole-stream mass
782 balance. *Water Resources Research*, 49(10), 6298–6316. https//doi:10.1002/wrcr.20492

783 Incropera, F.P., D.P. Dewitt, T.L. Bergman, & A.S. Lavine (2007), Fundamentals of Heat and
784 Mass Transfer, John Wiley, Hoboken, NJ.

785 Kessler, A.J., Glud, R.N., Cardenas, M.B., Larsen, M., Bourke, M.F., Cook, P.L.M. (2012),
786 Quantifying denitrification in rippled permeable sands through combined flume experiments and
787 modeling. *Limnology and Oceanography*, 57, 1217-1232.

788 Kessler, A.J. Glud, R.N., Cardenas, M.B., Cook, P.L.M. (2013), Transport Zonation Limits
789 Coupled Nitrification-Denitrification in Permeable Sediments. *Environmental Science and*
790 *Technology*, 47, 13404-13411.

791 Kirchner, J.W., Feng, X., Neal, C. (2000) Fractal stream chemistry and its implications for
792 contaminant transport in catchments. *Nature*, 403, 524-527.

793 Knapp, J.L.A., Gonzalez, Pinzon, R., Drummond, J.D., Larsen, L.G., Cirpka, O.A., & Harvey,
794 J.W. (2017), Tracer-based characterization of hyporheic exchange and benthic biolayers in
795 streams. *Water Resources Research*, 53, 1575-1594. https//doi:10.1002/2016WR019393

796 Knapp, J.L.A. & Kelleher, C. (2020), A Perspective on the Future of Transient Storage
797 Modeling: Let's Stop Chasing Our Tails. *Water Resources Research*, 56(3), e2019WR026257.

798 Kotz, S., & Nadaraj, S. (2000) "Extreme value distributions: theory and applications", World
799 Scientific, Singapore.

800 Leij, F.J., Priesack, E., Schaap, M.G. (2000), Solute transport modeled with Green's functions
801 with applications to persistent solute sources. *J. Contaminant Hydrology*, 41, 155-173.

802 Leray, S., Engdahl, N., Massoudieh, A., Bresciani, E., & Mccalum, J. (2016) Residence time
803 distributions for hydrologic systems: Mechanistic foundations and steady-state analytical
804 solutions. *J. Hydrology*, 543 (Part A), 67-87.

805 Marion, A., & Zaramella, M. (2005) Diffusive Behavior of Bedform-Induced Hyporheic
806 Exchange in Rivers. *ASCE J. Environmental Engineering*, 131, 1260-1266.

807 McCabe, W.L,., Smith, J.C., & Harriott, P. (2010) "Unit Operations of Chemical Engineering",
808 5th Ed. McGraw-Hill Inc, New Delhi.

809 O'Connor, B.L. & Harvey, J.W. (2008), Scaling hyporheic exchange and its influence on
810 biogeochemical reactions in aquatic ecosystems. *Water Resources Research*, 44, W12423.
811 https//doi:10.1029/2008WR007160

812 Perez Guerrero, J.S., Pontedeiro, E.M. van Genuchten, M.Th., Skaggs, T.H. (2013), Analytical
813 solutions of the one-dimensional advection-dispersion solute transport equation subject to time-
814 dependent boundary conditions. *Chemical Engineering Journal*, 221, 487-491.

815 Sabersky, R.H., & Acosta, A.J. (1989) "Fluid Flow: A First Course in Fluid Mechanics", 3rd Ed.,
816 Pearson College Div., New York, NY, USA.

817 Sawyer, A.H., & Cardenas, M.B. (2009) Hyporheic flow and residence time distributions in
818 heterogeneous cross-bedded sediment. *Water Resources Research*, 45, W08406.

819 Shen H.W., Fehlman H.M., Mendoza C. (1990), Bed form resistances in open channel flows, *J.*
820 *Hydraul. Eng. ASCE*, 116(6), 799-815, doi:10.1061/(ASCE)0733-9429(1990)116:6(799)

821 Stonedahl, S.H., Harvey, J.W., Wörman, A., Salehin, M., Packman, A.I. (2010), A multiscale
822 model for integrating hyporheic exchange from ripple to meanders. *Water Resources Research*,
823 46, W12539. doi: 10.1029/2009WR008865

824 Thibodeaux, L.J., & Boyle, J.D. (1987), Bedform-generated convective transport in bottom
825 sediment. *Nature*, 325, 341-343.

826 Tomasek, A.A., Barman, T.D., Wang, P., Kozarek, J.L., Staley, C., Sadowsky, M.J., & Hondzo,
827 M. (2018). The effects of turbulence and carbon amendments on nitrate uptake and microbial
828 gene abundances in stream sediment. *J. Geophysical Research: Biogeoscience*, 123, 1289-1301.
829 https//doi:10.1002/2017JG004261

830 Tufenkji, N., Elimelech, M. (2004), Correlation Equation for Predicting Single-Collector
831 Efficiency in Physicochemical filtration in Saturated Porous Media. *Environmental Science and*
832 *Technology*, 38, 529-536.

833 Vaux, W.G. (1968) Intragravel flow and interchange of water in a streambed. *Fishery Bulletin*
834 *66*, 479-489.

835 Voermans, J. J., Ghisalberti, M., & Ivey, G. N. (2017), The variation of flow and turbulence
836 across the sediment-water interface. *Journal of Fluid Mechanics*, 824, 413-437.
837 https//doi:10.1017/jfm.2017.345

838 Voermans, J. J., Ghisalberti, M., & Ivey, G. N. (2018), A model for mass transport across the
839 sediment-water interface. *Water Resources Research*, 54, 2799-2812.
840 https//doi:10.1002/2017WR022418

841 Wolke, P., Teitelbaum, Y., Deng, C., Lewandowski, J., Arnon, S. (2020), Impact of Bed Form
842 Celerity on Oxygen Dynamics in the Hyporheic Zone. *Water*, 12, 62.

843 Wörman, A., Packman, A., Johansson, I., & Jonsson, K. (2002) Effect of flow-induced exchange
844 in hyporheic zones on longitudinal transport of solutes in streams and rivers. *Water Resources*
845 *Research* 38(1), 2-1-2-15.

846 Wörman, A., Packman, A.I., Marklund, L., Harvey, J.W., & Stone, S.H. (2007), Fractal
847 topography and subsurface water flows from fluival bedforms to the continental shield.
848 *Geophysical Research Letters*, 34(7), L07402. https//doi:10.1029/2007GL029426

849 Yates, S.R. (1992), An analytical solution for one-dimensional transport in porous media with an
850 exponential dispersion function. *Water Resources Research*, 28(8), 2149-2154.

851
852

853 **Table 1**. A summary of the probability distributions trialed as potential descriptors of the

854 Bedform Pumping Model's residence time distribution and their inferred parameter values.

Distribution Name	PDF for the BPM's dimensionless residence time, $f_{\mathrm{RTD}}(\bar{\tau})$	Inferred Parameter Values	Kolmogorov Smirnov Test	
			Statistic	Rank
Fréchet	$\frac{\beta}{1-e^{-\beta/\mu}}\frac{e^{-\frac{\beta}{\mu+\bar{t}}}}{\left(\mu+\bar{t}\right)^2},\ \bar{t}\geq 0$	$\beta=1.6,\ \mu=0.2$	0.00881	1
Pareto	$\frac{\alpha k^{-1/\gamma}}{\gamma}\left(\bar{t}^{1/\gamma-1}\right)\left(1+\left(\frac{k}{\bar{t}}\right)^{-1/\gamma}\right)^{-(1+\alpha)},\ \bar{t}\geq 0$	$k=1.137,$ $\alpha=0.504,$ $\gamma=0.557$	0.01088	2
Log Normal	$\frac{e^{-\frac{(\ln\bar{t}-\mu)^2}{2\sigma^2}}}{\bar{t}\sqrt{2\pi\sigma^2}},\ \bar{t}\geq 0$	$\mu=0.891,$ $\sigma=1.405$	0.05547	3
Gamma	$\frac{\beta^{-\alpha}}{\Gamma\left[\alpha\right]}\bar{t}^{\alpha-1}e^{-\frac{\bar{t}}{\beta}},\ \bar{t}\geq 0$	$\alpha=0.267,$ $\beta=126.7$	0.30746	4
Exponential	$\lambda e^{-\lambda\bar{t}},\ \bar{t}\geq 0$	$\lambda=0.03$	0.62029	5

855

856

857